Fragmentation of relativistic gold by various target nuclei

C. J. Waddington, J. R. Cummings,* B. S. Nilsen,‡ and T. L. Garrard†
School of Physics and Astronomy, University of Minnesota, Minneapolis, Minnesota 55455
(Received 8 June 1999; published 20 January 2000)

We have studied the interactions of gold nuclei $^{197}_{79}$Au at eight different energies between 0.9 and 4.0 *A* GeV, in targets ranging in mass from hydrogen to lead. This paper combines the results of these studies with earlier measurements at higher and lower energies. We discuss the production of fragments with charges *Z* between 81 and 50. The systematic trends found have allowed us to improve previously developed empirical relations which predict the cross sections in any target or energy for the production of fragments with $77 \leqslant Z \leqslant 67$. Fragments with single and double charge pickup are observed in all targets at all energies. Fragments which have lost a single charge represent a special case, due presumably to the effects of electromagnetic dissociation. The energy variations of the total cross sections and the approach with increasing energy to limiting fragmentation are studied.

PACS number(s): 25.75.−q, 25.70.Kk, 27.80.+w

I. INTRODUCTION

When relativistic gold nuclei $^{197}_{79}$Au interact with target nuclei they frequently produce heavy fragments whose charge differs from that of the incident gold nucleus by a relatively small amount. The primary motivation for these studies was to determine the nuclear parameters needed for calculations of the propagation of very heavy cosmic ray nuclei through interstellar and local matter. The production of nuclei with charges changed from that of the incident projectile nucleus δZ for $+2 \leqslant \delta Z \leqslant -30$, has been studied in this work, using projectile nuclei with energies *E* between 0.9 and 4.0 *A* GeV. Our experimental techniques do not allow us to study fragments with larger values of $|\delta Z|$, multifragmentation, or any details of the mass changes that occur. We have previously studied these interactions using similar techniques at energies both lower and higher than those reported here [1–6]. These earlier studies were based on data obtained using projectiles of gold accelerated at the LBL Bevalac to energies $\leqslant 1.0A$ GeV, and gold of 10.6*A* GeV at the Brookhaven Alternating Gradient Synchrotron (AGS). The 10.6*A* GeV gold results were confirmed by the measurements of Hirzebruch *et al.* [7] using quite different detectors. Large differences were found between the partial cross sections for the production of each element, $\sigma(\delta Z, E, A_T)$, where A_T is the target mass, at high and low energies. A main goal of this work was to study the form of the energy dependence of these partial cross sections, and to attempt to establish the energy at which limiting fragmentation was reached. It is frequently suggested that the significant representation of the energy involved in nucleus-nucleus interactions should not be the energy per nucleon of the projectile, but the total energy available in the center of mass. This may well be true for central collisions, in which most or all of the nucleons of both nuclei are involved. However, it does not appear to be applicable in peripheral collisions of the sort expected to produce fragments with small charge loss. In such collisions not all the nucleons will be involved and the energy per nucleon appears to be the significant parameter. It will be shown in Sec. V C that the partial cross sections with heavy target nuclei for small $-\delta Z$ can be well represented by a power-law dependence on *E*, the energy per nucleon, for $E \leqslant 4.0A$ GeV, which is not a function of the target mass.

We have now completed a study of the production of fragments by gold nuclei with eight different energies between 0.9 and 4.0 *A* GeV, interacting in targets that range in mass from hydrogen to lead. These results have established the excitation functions for this process and suggest that limiting fragmentation is approached by 4.0*A* GeV, Sec. V A. The large number of partial cross sections measured in this work have allowed us to establish analytical fits to the variations with δZ, *E*, and A_T. These fits have been used to construct relations that can match the values of the measured cross sections with considerable accuracy and can predict those that have not been measured, Secs. V B and V C. In this new study we observe fragments with $Z = 80$, charge pickup, as before [4,6]. The improved statistics also provide definitive evidence for the direct production of thallium, $Z = 81$, double-charge pickup, although with cross sections of less than one mbarn.

II. EXPERIMENT

A schematic of the detector array is shown in Fig. 1. This array is essentially similar to that used previously to study the high-energy gold interactions [6]. The analysis is thus also very similar, apart from the additional steps taken to ensure that the incident nuclei were indeed gold nuclei and not fragments produced in the slabs of material placed in front of the array to reduce the energy. Incident nuclei passed through a series of ion chambers and Cherenkov counters. The ion chambers in front of the targets served to ensure that the nuclei selected for analysis were incident gold nuclei, not impurities in the beam, or fragments from interactions in the

*Present address: Washington University, St. Louis, Missouri 63130.
‡Present address: Van de Graff Laboratory, Ohio State University, Columbus, Ohio 43210.
†Deceased.

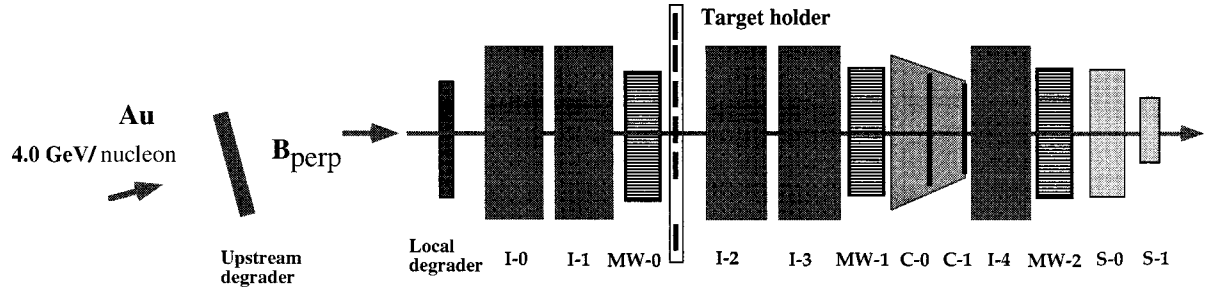

FIG. 1. Schematic of the detector array. Ion chambers I-0 to −4 are four gap parallel plate chambers filled with P10 gas. Cherenkov counters C-0 and −1 contain radiators of Pilot 425 plastic mounted in light diffusion boxes. The multiwire proportional counters MW −0 to −2 have 1 mm wire spacing. The target holder can place any of the targets in the beam by remote command. Local and upstream degraders were added as needed to reduce the beam energy. S-0 and S-1 were test detectors not used in this analysis.

energy degraders. Those detectors mounted behind the targets determined the charges of the nuclei that emerged; either fragments from interactions in the target material, or surviving gold nuclei. Details of the detectors and the general analysis have been described previously [2,6].

The AGS delivered nuclei to the array with an initial energy of 4.0*A* GeV. Local lead and external copper degraders were used to reduce the energy in the targets in a series of steps. The energy losses in the degraders were calculated using expressions for dE/dx appropriate for high charge particles introduced by Ahlen [9,10] and confirmed to within 2% by Waddington *et al.* [11]. Data on interactions were taken at energies E_{beam} of 4.0, 3.3, 2.7, 2.4, 2.0, 1.6, 1.2, and 0.92 *A* GeV. Energies were reduced from 4.0 to 2.0 *A* GeV by using local degraders placed immediately in front of the first detectors. These local degraders were then replaced by an external degrader placed in the beam line upstream to reduce the energy incident on the array to 2.0*A* GeV. The majority of the fragments produced in this degrader were swept out of the beam by downstream magnets before reaching our array. Only those fragments with rigidities within about 1% of that of the gold nuclei reached the array. These could be clearly identified and eliminated during the analysis. Excellent agreement between the results obtained at 2.0*A* GeV using either internal or external degraders, showed that any effects due to the unavoidable presence of lighter unstable isotopes of gold in the degraded beams was negligible. Still lower energies were obtained by combining the upstream degrader with additional local degraders.

At each energy, separate runs were made to take data on the interactions in targets of polyethylene (CH_2), carbon, aluminum, copper, tin, and lead. The thicknesses of these targets were chosen so that between 10 and 20 % of the incident nuclei would be expected to interact. In addition, data were taken with no target present, to evaluate the background corrections. Between 10^5 and 10^6 incident projectiles were recorded for each energy and target combination, see Table IV. Comparison of the results in the polyethylene and carbon targets allowed a determination of the cross sections in a pure hydrogen target. In practice, each set of runs was cycled through several times in order to increase the statistical weight and to ensure that complete sets had been obtained before the experiment was terminated by outside factors beyond our control. The results from these repeated runs could then be combined, since there were no significant long-term drifts in the responses of any of the detectors.

One of the most important characteristics of experiments such as these is the degree of charge resolution obtained. Figure 2 shows an individual charge spectrum for the case of 4.0*A* GeV gold nuclei in a polyethylene target. The charge resolution achieved in each run can be expressed in terms of the width of the gold peak, or the widths of the fragment peaks, measured in the detectors after the target. Table I lists the resolutions obtained at each energy, averaged over all targets, and shows that they are sufficient to resolve the high-Z fragments almost completely. Even those with $\delta Z = \pm 1$ can be clearly distinguished from the large gold peak. Fragments with $\delta Z < -20$ show reduced resolution due to the confusing effects of multiple fragments from a single interaction, but can still be resolved down to $\delta Z = -30$.

III. DETERMINATION OF TOTAL AND PARTIAL CROSS SECTIONS

Each detector, aside from the hodoscopes, produced two independent signals which should be identical, apart from

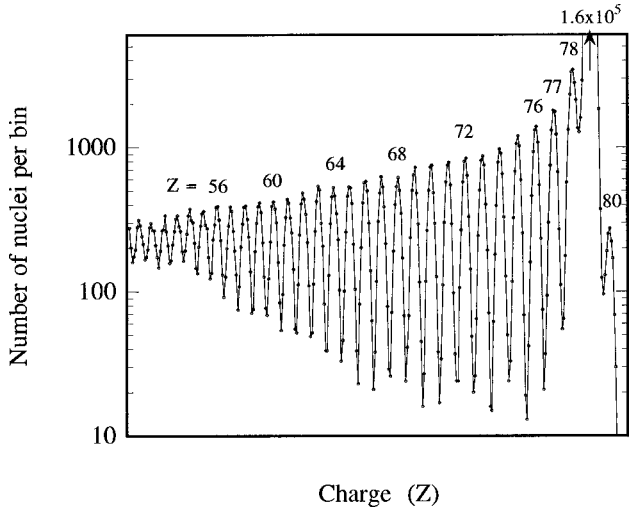

FIG. 2. A charge spectrum for gold at 4.0*A* GeV interacting in a polyethylene target. The four thallium fragments in this data set are not visible on this plot (see Table IV). The gold peak has a maximum at 1.6×10^5 nuclei.

TABLE I. Detector resolution at various beam energies. One standard deviation width is shown for the gold peaks and for those peaks of fragments with $-3 \geqslant \delta Z \geqslant -7$. The resolution for the pickup peak is expected to be similar.

Gold energy *A* GeV	Width of gold peak (in charge units)	Width of fragment peaks (in charge units)
0.92	0.148	0.188
1.2	0.132	0.141
1.6	0.119	0.131
2.0 (local)	0.112	0.124
2.0 (upstream)	0.111	0.124
2.4	0.108	0.121
2.7	0.111	0.125
3.3	0.108	0.125
4.0	0.106	0.125

random fluctuations. For the ion chambers, these signals come from two parallel layers of gas, and for the Cherenkov detectors from two interleaved groups of four phototubes observing each radiator. We selected events for further analysis where each pair of signals were within three standard deviations (scaled with signal size compared to a gold signal) of each other. This ensured consistency between the two signals from each detector and eliminated those few events affected by noise spikes and other random fluctuations.

The signals produced by gold nuclei in each detector did show small temporal variations due to changes in gas temperature, voltage, and ambient magnetic fields (from other large experiments sited nearby in the beam hall). Each signal was corrected by a time-dependent factor based on the variations in the mean of the peak signals of gold nuclei. Two factors were determined, one for the ion chamber signals and one for the Cherenkov signals. We determined these factors for each type of detector by selecting a sample of events for which all the signals in the other type of detector were within two standard deviations of the peak gold signal. Then we constructed a time series of histograms of signals in the individual detectors from each 10^5 successive events. The peak signals in these histograms defined the variation of each signal with time. The ion chambers' variations were dominated by variations in the temperature and gas flow rate during the runs, while the variations in the Cherenkov detectors were dominated by changing magnetic fields from other large active detectors in the experimental hall. These factors typically varied from about 0.95 to 1.05. Periods during which the factors varied abruptly were excluded from further analysis.

The signals in the Cherenkov detectors were corrected by a factor corresponding to the thickness of the radiators at the particle location found with the hodoscope, MW-1, just in front of the detectors. This factor ranged from 0.994 to 1.006. No positional corrections were needed for the ion chamber signals.

In order to determine absolute values for the cross sections we selected a subset of the total number of events that triggered our data collection system. The most important of these selections was based on the signals in the ion chambers in front of the target, I0 and I1. We accepted for further consideration only those events in which these signals, when combined, were within 2 standard deviations of the mean signal for gold nuclei. This roughly corresponded to 0.4 charge units, depending on the energy of the particles. We also selected for position in the hodoscope in front of the target. The location of each event's trajectory was required to be within the main beam spot (chosen by inspection of histograms of position, separately for each run) in both horizontal and vertical coordinates. These selections ensure that essentially all the events studied involved incident gold nuclei with the primary energy and mass defined at the accelerator's last bending magnet.

We used the hodoscope immediately in front of the target holder to impose a cut on the time taken for the signals to reach their peak values after the system trigger. The hodoscopes have the longest expected time to reach peak, and this cut removed a small fraction of events in which the signals were unusual, for example, events in which electronic noise happened to trigger a single amplifier, or two particles entered the detector array in a very short time interval. The vast majority of events in this fraction were also excluded by other cuts.

The incident number of gold nuclei for the purpose of determining cross sections for charge change was defined as the number of events satisfying all of these selection criteria. We then selected a subset of these events by requiring that the signals of the ion chamber in front (I2) and the sum of the signals of those behind the Cherenkov detectors (I3 and I4) were consistent. Each was required to be a similar fraction of the signal of gold, to within three standard deviations, or about 0.8 charge units, depending on the energy of the particles. This selection removes virtually all of the events in which a particle changed charge by more than one due to an interaction in the material of the Cherenkov detector. It does not remove all of the events in which the charge changed by one.

We created a histogram of the remaining events as a function of the weighted sum of the signals of the detectors behind the target. In order to find the number of nongold nuclei that were created in the target and not in the material of the detectors, we subtracted from each target's histogram a scaled histogram of a run with no target and a similar energy at the detectors. Finally, we obtained the number of events in each peak by a fit to a Gaussian distribution, e.g., see Fig. 2. This number is then the number of nuclei considered to have undergone a charge change in the target and to have undergone no further charge changes in the material of the detectors.

Two further corrections for such charge changes were necessary to obtain the cross section for interaction in a thin target. First, we multiplied the number of events by a factor equal to the ratio of number of events with a signal corresponding to gold in the ion chambers in front of the Cherenkov detectors to the number of events with a signal corresponding to gold in the ion chambers in back of the Cherenkov detectors. This factor allows for the loss of gold nuclei that interact in the detectors. We used the result to

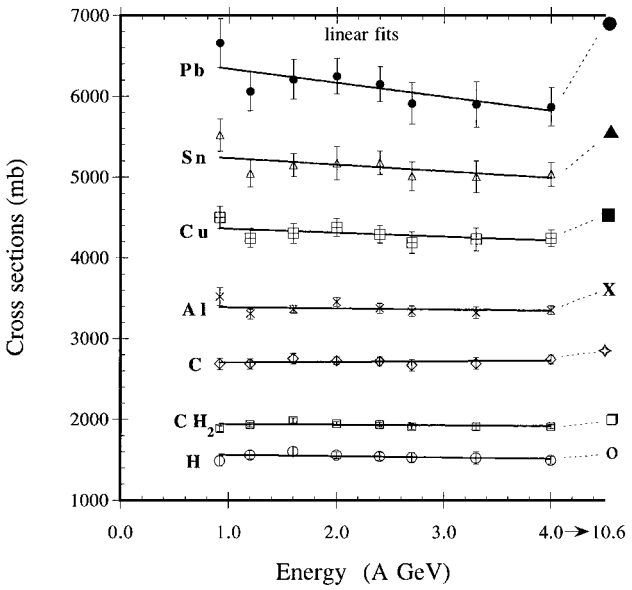

FIG. 3. Total charge changing cross sections Σ_T for gold nuclei in all targets as a function of beam energy. Note break in energy scale between 4.0 and 10.6 *A* GeV. Linear fits are shown for the values between 0.9 and 4.0 *A* GeV.

compute a preliminary estimate of the cross sections for production of nuclei with each value of δZ. Second, we performed an iterative calculation to correct for those nuclei which suffered a subsequent charge-changing interaction in the target. For this correction, we considered the thick target as a stack of thin slabs, and calculated the number of existing gold and fragment nuclei in each slab. We iterated the calculation, changing the preliminary cross sections until the results matched the numbers leaving the target.

Due basically to the relatively thin targets and the excellent charge resolution in all but the lowest energy runs, systematic uncertainties are in all cases significantly smaller than statistical. These systematic uncertainties are reduced by ensuring that the runs with no target had adequate statistical weight.

IV. RESULTS

A. Total cross sections

The total charge changing cross sections Σ_i were measured at each energy and in each target. The cross sections in hydrogen were calculated from the carbon (C) and polyethylene (CH_2) targets using the relation

$$\Sigma_{\mathrm{H}} = 0.5(3\Sigma_{\mathrm{CH_2}} - \Sigma_{\mathrm{C}}), \tag{1}$$

noting that $\Sigma_{\mathrm{CH_2}}$ is the averaged nuclear cross section for CH_2, defined as the cross section per molecule divided by 3.

The energy dependence of Σ_i is shown in Fig. 3 for all targets, together with linear fits between 0.9 and 4.0 *A* GeV of the form

$$\Sigma = \Sigma_0 + \gamma \cdot E_{\mathrm{beam}}. \tag{2}$$

The values of Σ_0 and γ are given in Table II.

TABLE II. Values of constants from linear fits, Eq. (2), to variations with energy of total cross sections for all targets.

Target	Σ_0 (mb)	$\pm$	γ	$\pm$	χ^2
Pb	6512	228	−172	92	0.43
Sn	5316	149	−81	59	0.62
Cu	4408	107	−48	42	0.47
Al	3399	57	−12.9	22.3	0.93
C	2696	55	8.2	22.1	0.23
CH_2	1950	26	−7.4	10.7	1.08
H	1577	48	−15.7	19.5	0.46

Note that the earlier measurements at the Bevalac with $E < 0.92A$ GeV [1–3] did not determine values of Σ_i. It can be seen from these new results that Σ_i is essentially constant for the lighter targets, but that for the heavier targets there is a small but significant decrease in Σ_i as E increases to 4.0*A* GeV. This decrease in Σ_i does not continue out to 10.6*A* GeV. Instead, there are increases, which are greatest for the heaviest targets. These increases at high energy could be attributed to the increasing importance of electromagnetic dissociation (EMD), which was discussed in some detail previously by Geer *et al.* [6]. However, the increases for the heaviest targets appear to be larger than predicted by this earlier analysis. For example, Σ_{Pb} increases by about 1000 mb between 4.0 and 10.6 *A* GeV, whereas the analysis by Geer *et al.* [6] suggested that the contribution due to EMD at 10.6*A* GeV was only 310 mb. This suggests that either the magnitude of the EMD contribution, which was based on arguments involving factorization, has been underestimated, or that the nuclear cross sections increase with energy and mass number. Neither explanation is attractive and further data is needed to study this question in more detail.

The variation of Σ_i with the mass number of the target A_T is shown in Fig. 4. This figure shows all the data for each energy and power-law fits in A_T. Values for the two extreme cases are shown. The dependence closely follows, but is not exactly equal to, an $A_T^{1/3}$ relation. Such a relation would im-

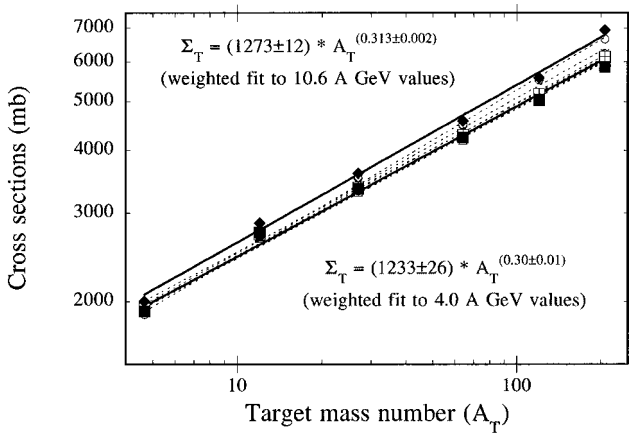

FIG. 4. Dependence of total charge changing cross sections Σ_T on target mass number A_T. Power-law fits are shown to values at 10.6 and 4.0 *A* GeV. Other energies are shown by dashed lines.

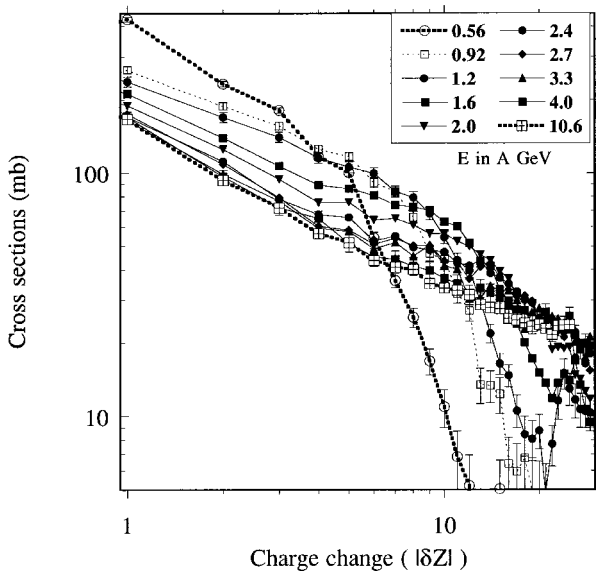

FIG. 5. Partial cross sections σ in mb, for gold on a hydrogen target, as a function of charge change $|\delta Z|$ at all available energies.

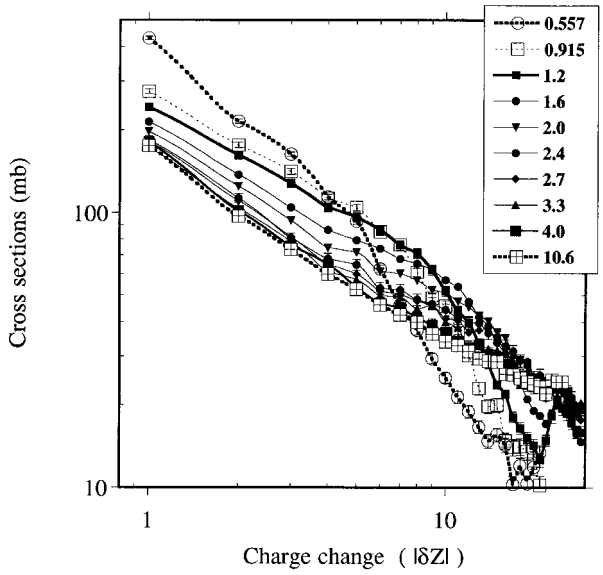

FIG. 6. Partial cross sections σ in mb, for gold on a polyethylene target, as a function of charge change $|\delta Z|$ at all available energies.

ply that Σ_i depends on the impact parameter between the two nuclei. However, it should be noted that this power-law relation would not extrapolate correctly to a hydrogen target, but would predict an value appreciably smaller than is measured. The good representation of the dependence on A_T by a power law suggests that it is reasonable to predict the cross sections for projectiles other than gold by scaling by an $A^{1/3}$ term, at least for A_P values that are not too dissimilar from that of gold.

The effects of EMD on the cross sections at the highest energy, 10.6*A* GeV, can be removed following the same procedure adopted before [6]. These reductions make minimal changes in the power-law fit to A_T. The power-law exponent at 10.6*A* GeV is reduced from 0.313 ± 0.002 to 0.303 ± 0.002, which brings it into agreement with the exponent of 0.299 ± 0.007 at 4.0*A* GeV.

B. Partial cross sections

1. Hydrogen

The hydrogen cross sections have been discussed in detail in a recent publication [8]. In that paper the emphasis was on the astrophysical significance of these cross sections to the problem of the propagation of heavy cosmic ray nuclei through the interstellar medium. Here we will concentrate on a comparison of the systematics of these cross sections with those on heavier targets.

The elemental partial cross sections σ for the production of fragments with δZ from $+2$ to -30, were measured at each energy and in each target. The values for σ in hydrogen were then calculated using the partial cross section version of Eq. (1), with the appropriate values of σ measured in CH_2 and C.

The values of σ for negative values of δZ at the different energies as a function of $|\delta Z|$ for carbon, polyethylene, and hydrogen targets are shown in Figs. 5–7. Also shown in these figures are the low-energy data from Cummings *et al.* [2], and the high-energy data from Geer *et al.* [6]. These plots are on log-log scales, with the new results shown as solid symbols and the previous data as open symbols. These plots, while very busy, illustrate the general power-law nature of the relation between σ and $|\delta Z|$ for a relatively heavy target like carbon, and the deviations from a power law for the lighter targets and the lower energies.

Examination of Figs. 5–7 show the considerable energy dependence of σ, particularly for a hydrogen target. There are obviously very large changes for those fragments with $|\delta Z| > 10$. However, the σ's for the production of these

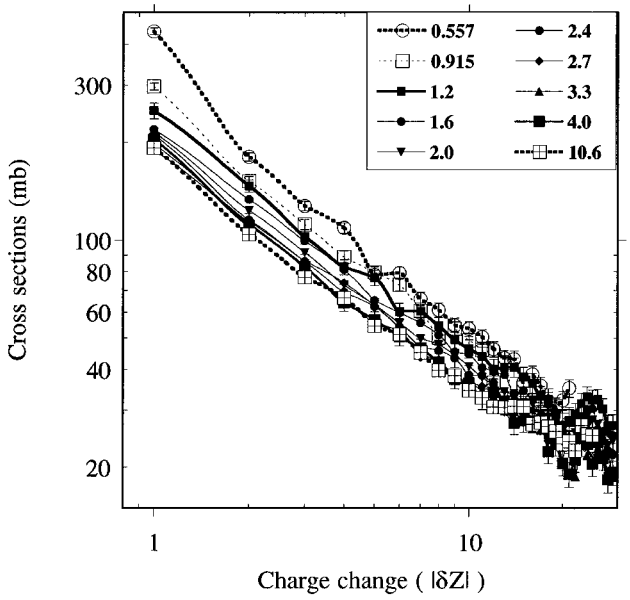

FIG. 7. Partial cross sections σ in mb, for gold on a carbon target, as a function of charge change $|\delta Z|$ at all available energies.

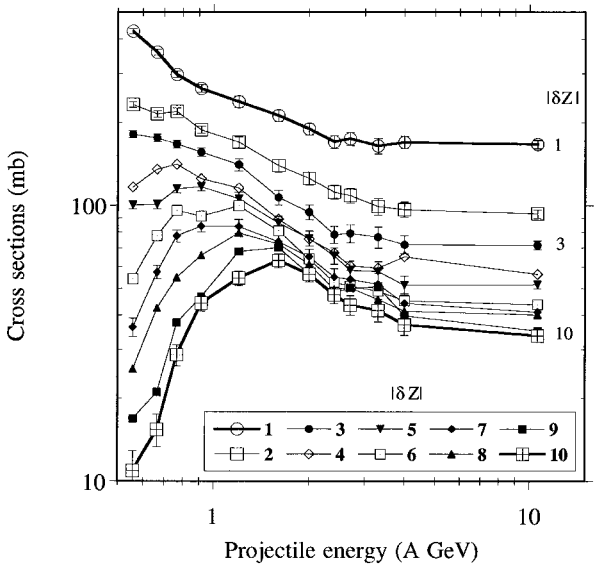

FIG. 8. Partial cross sections σ in mb, for gold on a hydrogen target, as a function of beam energy for different fragments with $|\delta Z|$ between 1 and 10.

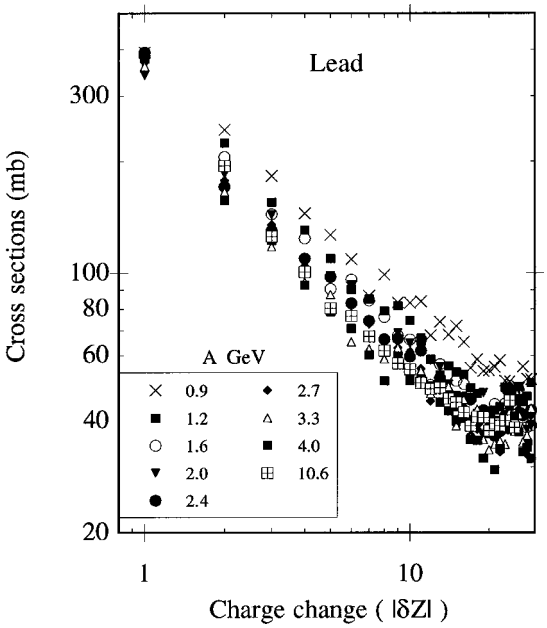

FIG. 9. Partial cross sections σ in mb, for gold on a lead target, as a function of charge change $|\delta Z|$ at all available energies, listed in A GeV.

lighter fragments are all relatively small, and hence, comparatively unimportant to the propagation problem. The significant σ's are those for the fragments with $|\delta Z| \leqslant 10$. The values of σ for each of these δZ are shown as a function of the projectile energy in Fig. 8. A This figure shows that in general for small δZ, σ_H decreases with increasing E, but that for large δZ, σ_H reaches a maximum at an intermediate energy. As might be expected, at low energies the production of fragments decreases rapidly as $|\delta Z|$ increases. At higher energies, this effect becomes less important, and σ only decreases slowly as $|\delta Z|$ increases. For each δZ, σ shows a dependence on energy that becomes less and less marked as the energy increases, although for some δZ there is still a indication of a small decrease between the two highest energies. For most purposes, it is reasonable to assume that limiting fragmentation has been reached by 4.0A GeV (see Sec. V A).

2. Heavy targets

The partial cross sections in heavy targets show similar features to those in carbon, Fig. 7. As an example, the variations of σ with $|\delta Z|$ for the Pb target are shown in Fig. 9. In all the heavy targets there are good power-law relationships between σ and δZ, at least for $|\delta Z| < 20$. It can also be seen that, although there is a dependence on energy, it is much less than that observed for the hydrogen targets.

V. ANALYSIS

The large body of data that has now been collected on the production of fragments in these relativistic interactions of heavy nuclei in various target materials can be used to address a number of interesting topics. The problem of whether the regime of limiting fragmentation has been reached in these experiments is discussed in the next section. The following sections discuss the derivation of relations allowing the prediction of partial cross sections for any target or energy. These new relations are compared with those derived previously [5] from a more limited data set. Since the major cross sections are for $|\delta Z| \leqslant 12$ and since it is only these large fragments that are significant in propagation calculations, attention has been directed mainly to predicting the production of these fragments.

A. Limiting fragmentation

We can study whether the regime of limiting fragmentation has been reached in this range of energies by looking at the changes in the cross sections between the two highest energies. Consider the ratio

$$R(\delta Z, A_T) = \sigma_{10}(\delta Z, A_T)/\sigma_E(\delta Z, A_T), \tag{3}$$

where for each target R is a function of δZ, and σ_{10} and σ_E are the partial cross sections at 10.6A GeV and at a lower energy E, for each value of δZ. In the case that true limiting fragmentation has been established by E A GeV, $R(\delta Z)$ should equal 1.0 within the experimental uncertainties for each target. Figure 10 shows a plot for $E = 4.0$, 3.3, and 2.7A GeV, of the mean values of R averaged over $\delta Z = -1$ to -12 for each of the targets, together with the standard deviations on these means. It can be seen that there may be an apparent mass dependence for $\langle R \rangle$. With $E = 4A$ GeV, R is marginally less than unity for the lightest targets, while for the heaviest targets $\langle R \rangle$ appears to be consistent with unity, although with a large uncertainty. As E decreases, R becomes smaller, particularly for the lighter targets. Examination of the variation of $R(E=4)$ with δZ for a hydrogen target, shows that these deviations from unity for each δZ are small, Fig. 11. For lead it appears that the apparent increase in $\langle R \rangle$ is due to the high values of $R(\delta Z = -1)$ and

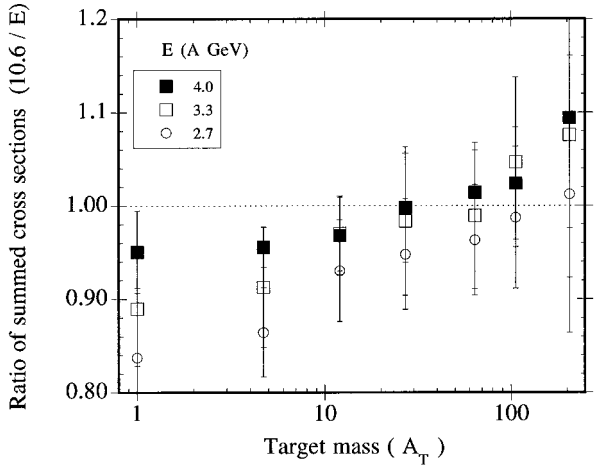

FIG. 10. Plot of the ratio $R(10.6/E)$, see Eq. (3), averaged over $1 \leqslant |\delta Z| \leqslant 12$, between 10.6 and 4.0, 3.3, and 2.7 A GeV, as a function of target mass A_T.

$R(\delta Z=-2)$, which can partially be attributed to the effects of EMD at high energies. For $|\delta Z| \geqslant 3$, the R values are consistent with unity.

It appears reasonable to conclude that, in general, limiting fragmentation has been reached between 4.0 and 10.6 A GeV for gold nuclei.

B. Partial cross sections

The variations of the partial cross sections for $E \leqslant 5.0A$ GeV in all the targets and for $|\delta Z| \leqslant 12$, can be fitted by one or two power-law relations in energy, depending on the target and δZ:

$$\sigma(\delta Z,E,A_T)=\sigma_0(\delta Z,A_T)\cdot E^{n(\delta Z,A_T)} \text{ mb}, \tag{4}$$

where $\sigma_0(\delta Z,A_T)$, is the value of the cross section at $1.0A$ GeV, and $n(\delta Z,A_T)$ is the exponent of the energy variation. For a hydrogen target, these parameters also depend on a critical energy E_c representing a transition from a positive to a negative exponent.

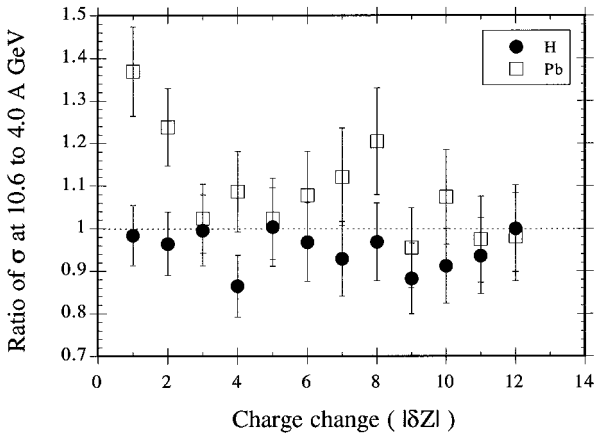

FIG. 11. Values of $R(10.6/4.0)$ as a function of charge change $|\delta Z|$ in hydrogen and lead targets.

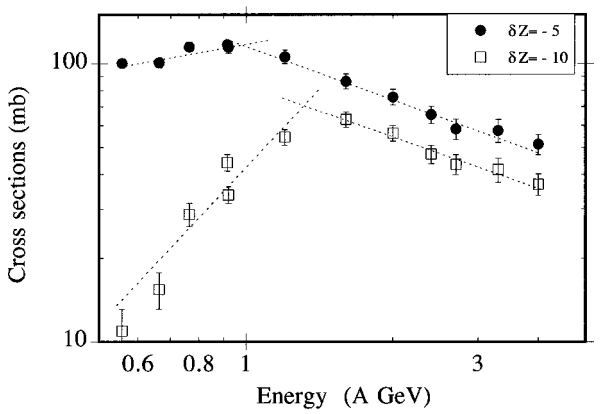

FIG. 12. Partial cross sections σ in mb, for gold on a hydrogen target, for two values of δZ (-5 and -10) as a function of energy. Power-law fits of the type in Eq. (4) are shown for each section of the data.

1. Hydrogen cross sections

For hydrogen and $|\delta Z|>3$ it appears that E_c increases slowly from 1.0 to 1.3 A GeV as δZ increases. Examples of the relatively abrupt change in form seen in the hydrogen cross sections are shown in Fig. 12 for $\delta Z=-5$ and -10. For $E_c \leqslant E \leqslant 5.0$ or for $|\delta Z| \leqslant 3$, both σ_0 and n can be represented as power laws in δZ of the form

$$\sigma_0=(267\pm 3)\cdot|\delta Z|^{(-0.553\pm 0.012)} \text{ mb}, \tag{5}$$

$$n=(-0.452\pm 0.019)\cdot|\delta Z|^{(0.143\pm 0.033)}. \tag{6}$$

At $E<E_c$ and $|\delta Z| \geqslant 4$, σ_0 and n can both be represented by relations of the form

$$\sigma_0=(359\pm 14)\cdot\exp(|\delta Z|(-0.217\pm 0.005)) \text{ mb}, \tag{7}$$

$$n=(4.79\pm 0.29)\cdot\ln(|\delta Z|(0.26\pm 0.009)). \tag{8}$$

It can be seen that the change in behavior at the critical energy is drastic. The exponent of the energy dependence varies from being positive at low energies to negative at higher energies. In all the fits to the data and to the power-law parameters there are acceptable values of χ^2 for each of the individual fits. A comparison between all the measured cross sections in hydrogen and those predicted from Eqs. (4)–(8) is shown in Fig. 13. It is found that 80% of the predictions are within 15% of the measured values. Alternatively, 42% of the predictions are within one standard deviation of the measured values and 74% are within two standard deviations.

For $|\delta Z|>12$ it is necessary to increase E_c to $1.8A$ GeV in order to obtain acceptable power fits. For $E>E_c$ there are drastic changes in the forms of both σ_0 and n from the values for lower δZ. For example, Fig. 14 shows the exponent parameter n at high energy, $4.0A$ GeV, as a function of δZ, together with the fit for $|\delta Z| \leqslant 12$.

A comparison of the results from these predictions and those obtained from the revised version derived in earlier work [5], shows that this new formalism is significantly bet-

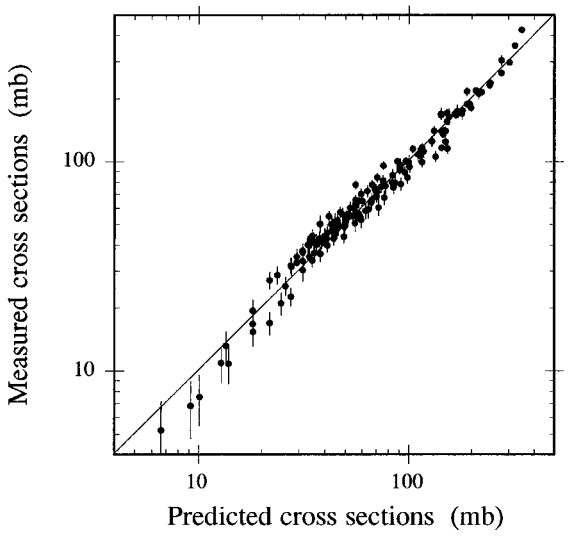

FIG. 13. Comparison between measured partial cross sections of gold in hydrogen for δZ between -1 and -12 and the values predicted from Eqs. (4) to (8).

ter at matching the available measured values. Using the present predictions, 91% of the values agree to within 20% of the measured values for $2 \leqslant |\delta Z| \leqslant 12$. The previous formalism, which was limited to fewer energies but with more projectile types, was only able to match 76% of a data set to within 20%.

2. Heavy target cross sections

For the targets heavier than hydrogen, it is not necessary to invoke a critical energy. All the cross sections for $2 \leqslant |\delta Z| \leqslant 12$ and $E \leqslant 5.0A$ GeV for each target can be fitted by one power law, although with individual values of $\sigma_0(\delta Z, A_T)$ and $n(\delta Z, A_T)$, similar to Eq. (4). The values of σ_0 and n can in turn be described by power laws in $|\delta Z|$ of the form

$$\sigma_0(\delta Z, A_T) = \alpha(A_T) \cdot |\delta Z|^{\beta(A_T)} \text{ mb}, \tag{9}$$

$$n(\delta Z, A_T) = \gamma(A_T) \cdot |\delta Z|^{\chi(A_T)}. \tag{10}$$

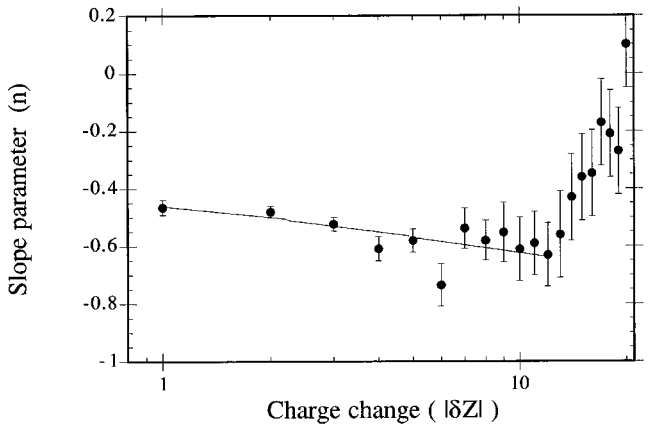

FIG. 14. Values of exponent parameter from Eq. (4) as a function of charge change $|\delta Z|$ for gold on hydrogen at 4.0A GeV.

TABLE III. Values of constants in Eqs. (9)–(14).

Constant	Value	±	Constant	Value	±
ϕ	196	5	a	-0.253	0.014
ε	0.108	0.008	b	$-(0.6\times10^{-4})$	(5×10^{-4})
θ	-0.788	0.017	c	-0.143	0.034
τ	-0.017	0.007	d	(4×10^{-4})	(5×10^{-4})

Finally, α and β can be described by power laws in A_T, and γ and χ as linear relations in A_T:

$$\alpha(A_T) = \phi \cdot A_T^{\varepsilon}, \tag{11}$$

$$\beta(A_T) = \vartheta \cdot A_T^{\tau}, \tag{12}$$

$$\gamma(A_T) = a + b \cdot A_T, \tag{13}$$

$$\chi(A_T) = c + d \cdot A_T. \tag{14}$$

The fitted values of these various constants with their uncertainties are given in Table III.

Examination of these values shows that β, γ, and χ are nearly independent of A_T. The resultant global fit to the data is then given by

$$\sigma(\delta Z, E, A_T) = (\phi A_T^{\varepsilon}) \cdot |\delta Z|^{\vartheta A_T^{\tau}} \cdot E^{(a+bA_T)\cdot|\delta Z|^{(c+dA_T)}} \text{ mb}. \tag{15}$$

Application of this global fit to all the available data for $2 \leqslant |\delta Z| \leqslant 12$ and $0.5 \leqslant E \leqslant 10.6A$ GeV shows that the fit is a good representation of the data. Figure 15 shows a histogram of the ratio of the predicted to the measured cross sections for the 627 cross sections. 60% of all the predictions are within 5% of the measured values, 88% are within 10%. Alternatively, 65% of the predictions are within one standard deviation of the measured values and 93% are within two standard deviations. Given the uncertainties in the constants of Table III, the predictions appear to be excellent. Note that these predictions are significantly better than those derived above for the hydrogen target.

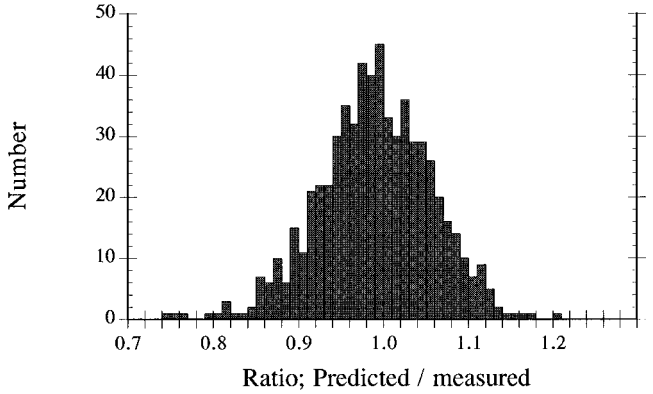

FIG. 15. Histogram of ratio of predicted to measured partial cross sections for all targets carbon and heavier. All energies 0.5A GeV and above, $2 \leqslant |\delta Z| \leqslant 12$. Note does not include values for $\delta Z = -1$.

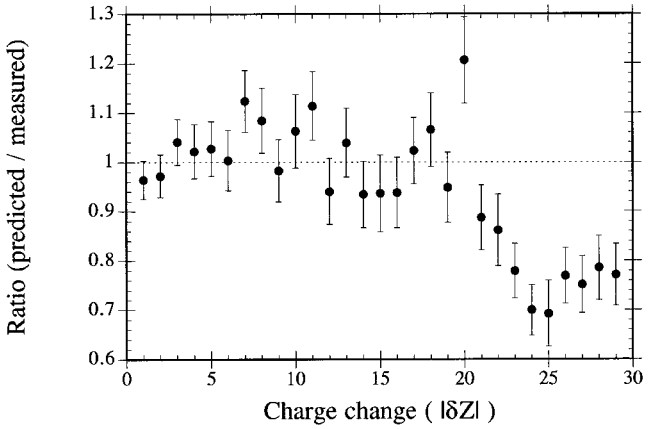

FIG. 16. Plot of ratio of predicted to measured cross sections for gold on aluminum at 4.0*A* GeV, as a function of charge change $|\delta Z|$.

If we neglect those terms with small constants then

$$\sigma(\delta Z,E,A_T)\approx(196\cdot A_T^{0.1})|\delta Z|^{-0.8}\cdot E^{(0.25)\cdot\delta Z^{-0.15}}\ \text{mb}. \tag{16}$$

From this form we note that σ is only weakly dependent on A_T, but does show a clear dependence on E for $E \leqslant 4.0A$ GeV when $|\delta Z|\leqslant 12$. Thus

$$\sigma(\delta Z,E,A_T)\propto A_T^{0.1};\propto|\delta Z|^{-0.8};\propto E^{-0.25\cdot\delta Z^{-0.15}}$$

$$\text{for } E\leqslant 4.0A \text{ GeV and } 2\leqslant|\delta Z|\leqslant 12.$$

The E dependence is not a function of A_T, showing that it is not appropriate to consider the total energy in the center of mass as an organizing variable in these peripheral interactions.

If we attempt to extend this global fit to those cross sections for fragments with $|\delta Z|>12$ we find that there is a reasonable representation for $|\delta Z|\leqslant 20$. An example is shown in Fig. 16 for Al at 4.0*A* GeV. Clearly, the predictions seriously underestimate the cross sections for $|\delta Z|>20$. This must at least be partially due to the effects of fission of the gold nuclei, which has been shown to be strongly energy dependent [12]. Symmetric fission (40,39) results in an apparent fragment with $\delta Z\approx -23$, while asymmetric fission (20,59) appears at $\delta Z\approx -17$. Such events will increase the apparent cross sections and result in the measured cross sections being larger than those for the production of a single fragment. Examination of Fig. 7 shows the increasing cross sections in carbon for $|\delta Z|$ in the low 20's that reflect the effects of fission. However, even for $|\delta Z|\leqslant 20$ the global fit is not as satisfactory as for the lower $|\delta Z|$ values. Figure 17 shows a histogram of the ratio of the predicted to measured cross sections for $13\leqslant|\delta Z|\leqslant 20$, for all heavy targets and energies. There is a consistent underestimation of the cross sections by rather less than 10% on average. Since these cross sections are small compared to those for small $|\delta Z|$, a failure to predict them as precisely is unlikely to have any significant effects on propagation calculations.

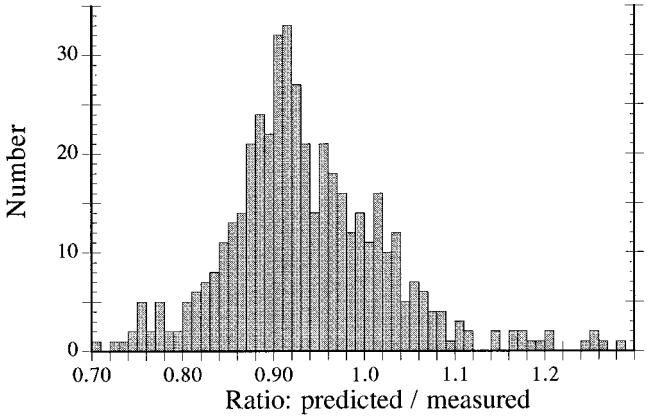

FIG. 17. Histogram of ratio of predicted to measured partial cross sections for all targets carbon and heavier. All energies 0.5*A* GeV and above, $13\leqslant|\delta Z|\leqslant 20$.

C. Minus 1 cross sections

The cross sections for those fragments that have lost just one charge are not well described by the global fit derived above. In general, the measured cross sections are significantly greater than those predicted. Examination of the cross sections for each target as a function of energy, Fig. 18, shows significant changes from the simple power-law relations at both the highest and lowest energies. At low energies this presumably is a reflection of the lack of total energy available to remove more than a single proton from the gold nucleus. At high energy the effects of EMD become noticeable [6]. In both cases these effects are largest for the heaviest targets, as could be expected.

D. Plus 1 cross sections

In each run it was possible to identify a clear peak of $_{80}$Hg nuclei, resulting from a single charge pickup, ''plus 1's.'' In most runs it was also possible to distinguish a small number

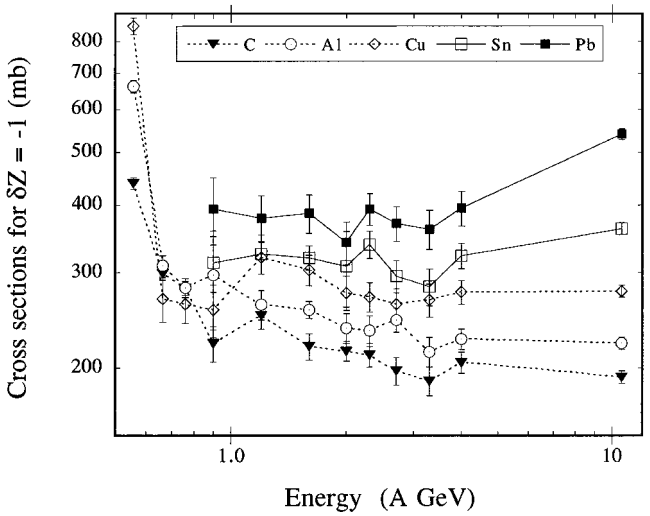

FIG. 18. Partial cross sections for $\delta Z=-1$ in heavy targets, as a function of energy. Values for each target are connected to guide the eye.

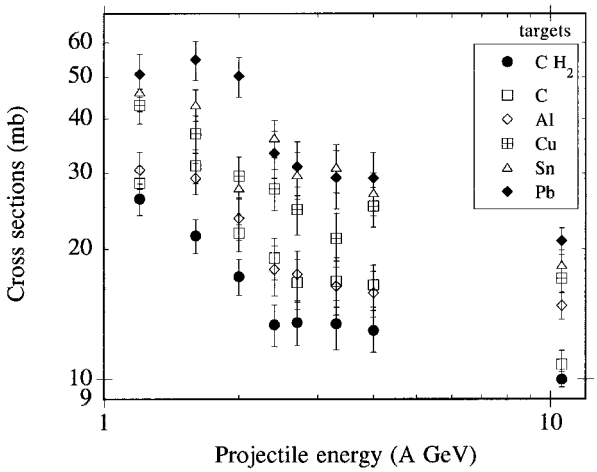

FIG. 19. Cross sections, in mb, for the production of $_{80}$Hg nuclei from $_{79}$Au nuclei in all targets, as a function of energy.

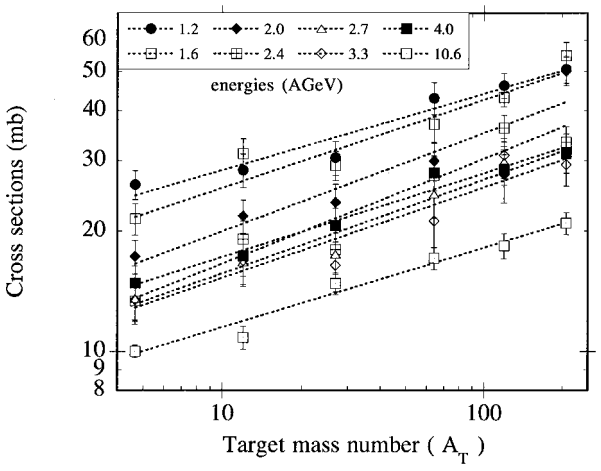

FIG. 20. Cross sections, in mb, for the production of $_{80}$Hg nuclei from $_{79}$Au nuclei at various energies, as a function of target mass number *A*. Power-law fits of the type of Eq. (17) are shown at each energy.

of $_{81}$Tl nuclei, double-charge pickup, ''plus 2's.'' The one exception was for the runs at 0.92*A* GeV, which had the worst charge resolution. The numbers of Hg and Tl fragments detected in all the runs with $E>1.0A$ GeV are given in Table IV, together with the cross sections deduced for the production of Hg after allowing for interactions in the lower detectors. The numbers of Tl nuclei that could be expected from secondary interactions of Hg nuclei in the targets were calculated assumed that the cross sections for producing Tl from Hg was the same as that for producing Hg from Au. Between 10 and 20 % of the observed Tl nuclei could have been produced in such successive pickup interactions. The clear excess of observed Tl nuclei over the estimates for secondary production indicated that there must be a mechanism for the direct production of nuclei that gain two charges in an interaction.

Our previous studies of charge pickup [4,6] involved a number of different projectiles and targets, but apart from one series of runs using gold nuclei with 10.6*A* GeV, was confined to energies of less than 1.5*A* GeV. These new results are limited to a single projectile, but cover a range of energies between those previously available. In addition, the targets used cover a wider range than was generally used previously.

The variation of these cross sections with energy is illustrated in Fig. 19, which shows all the data obtained in this experiment, together with the previous high-energy results. It can be seen that the cross sections decrease quite rapidly with increasing energy between 1.2 and 2.3 *A* GeV, and then appear to become almost constant up to 4.0*A* GeV. This fall in the cross sections with increasing energy is consistent with that reported for the pickup cross sections of ^{228}U [12]. There is apparently a further small, but significant decrease in the cross sections between 4.0 and 10.6 *A* GeV. Since the total charge changing cross sections are almost constant, the fraction of interactions producing Hg nuclei shows a similar energy dependence to that seen in Fig. 19. This fraction varies between 1.35 and 0.3 %, being highest in polyethylene and least in lead. In addition, it is clear that the cross sections do depend on the mass number of the target.

The earlier high-energy results were found to be well fitted by a power-law dependence on the target mass number A_T of the form

$$\sigma_{+1}=\mu(A_T)^{\kappa}. \tag{17}$$

In these previous fits, values for a hydrogen target deduced from the cross sections in carbon and polyethylene were included. In the present analysis, we have confined our results to the directly measured cross sections. The results of power-law fits, weighted by the experimental uncertainties, are shown in Fig. 20. Here the cross sections are plotted as a function of A_T for eight different energies of the gold nuclei. The values of the exponent coefficient κ and intercept coefficient μ for the plus 1's are shown as a function of energy in Figs. 21(a) and 21(b). The intercept μ is seen to fall steadily with increasing energy between 1 and 2.5 *A* GeV and then become essentially constant at higher energies, although there may be a slow decrease with energy. The power dependence κ is consistent, within the uncertainties, with being constant with energy, and reflects a rather weak dependence on A_T. It should be noted that this constancy was not apparent at energies less than 1.0*A* GeV [3], where κ decreased sharply and a power-law fit became less satisfactory. The fits to the data reported here had reduced χ^2 values with a mean of 1.09, showing that a power representation is acceptable. It has been suggested [12,13] that these cross sections should instead be fitted by a linear relation of the form

$$\sigma_{+1}=\delta[A_T^{1/3}+A_p^{1/3}-0.75(A_T^{-1/3}+A_p^{-1/3})] \tag{18}$$

originally proposed to represent single nucleon removal interactions [11]. However, applying Eq. (18) leads to reduced χ^2 values with a mean of 2.83, showing that it is not as good

TABLE IV. Numbers of incident gold and produced mercury and thallium nuclei in each target at each energy. Also percentage ratios of Hg/Au nuclei and cross sections for production of Hg.

Target	Energy (A GeV)	Gold $Z=79$	Mercury $\delta Z=+1$ $Z=80$	Mercury/gold %	Thallium $\delta Z=+2$ $Z=81$	Mercury (mb)
CH2	0.92	549 865	2246	0.408	15	40.1±2.7
CH2	1.2	677 551	1810	0.267	11	26.1±3.2
CH2	1.6	606 394	1329	0.219	15	21.5±6.1
CH2	2	1 016 661	1792	0.176	11	17.3±5.4
CH2	2.4	653 505	890	0.136	3	13.4±8.3
CH2	2.7	510 195	704	0.138	6	13.5±11.2
CH2	3.3	208 545	286	0.137	3	13.5±2.2
CH2	4	758 697	1003	0.132	4	13.0±2.7
C	0.92	265 343	535	0.202	3	35.4±3.0
C	1.2	332 145	539	0.162	3	28.4±4.0
C	1.6	291 779	519	0.178	3	31.2±4.6
C	2	607 879	756	0.124	11	21.8±5.8
C	2.4	350 532	381	0.109	2	19.1±1.9
C	2.7	244 360	233	0.095	0	16.7±2.8
C	3.3	233 817	225	0.096	1	16.9±2.4
C	4	388 740	366	0.094	3	16.5±3.7
Al	0.92	42 660	136	0.319	3	48.7±3.6
Al	1.2	216 822	434	0.200	4	30.5±5.7
Al	1.6	490 641	926	0.189	9	28.8±1.7
Al	2	200 126	309	0.154	3	23.6±2.1
Al	2.4	164 246	193	0.118	1	18.0±2.6
Al	2.7	188 591	216	0.115	1	17.5±3.2
Al	3.3	152 519	164	0.108	2	16.4±5.0
Al	4	288 463	299	0.104	6	15.9±5.2
Cu	0.92	282 294	556	0.197	3	69.3±1.5
Cu	1.2	404 781	496	0.123	3	43.0±2.1
Cu	1.6	357 277	376	0.105	3	37.0±2.4
Cu	2	354 919	298	0.084	0	29.5±3.0
Cu	2.4	390 826	306	0.078	1	27.6±3.6
Cu	2.7	311 719	219	0.070	2	24.7±4.2
Cu	3.3	280 340	169	0.060	0	21.2±1.6
Cu	4	470 655	336	0.071	2	25.1±2.2
Sn	0.92	341 775	791	0.231	1	122.9±2.3
Sn	1.2	508 699	444	0.087	4	46.2±3.2
Sn	1.6	969 544	789	0.081	6	43.2±3.7
Sn	2	183 827	96	0.052	0	27.7±4.4
Sn	2.4	575 610	392	0.068	4	36.2±1.8
Sn	2.7	467 333	262	0.056	2	29.8±2.2
Sn	3.3	374 170	218	0.058	4	30.9±2.3
Sn	4	602 846	306	0.051	1	27.0±3.0
Pb	0.92	337 026	614	0.182	3	145.6±4.0
Pb	1.2	564 934	360	0.064	1	50.8±4.5
Pb	1.6	535 712	368	0.069	1	54.8±1.4
Pb	2	545 319	343	0.063	5	50.2±1.9
Pb	2.4	637 275	266	0.042	1	33.4±1.9
Pb	2.7	548 070	213	0.039	2	31.0±2.7
Pb	3.3	455 235	167	0.037	3	29.3±3.1
Pb	4	481 736	176	0.037	1	29.2±4.3

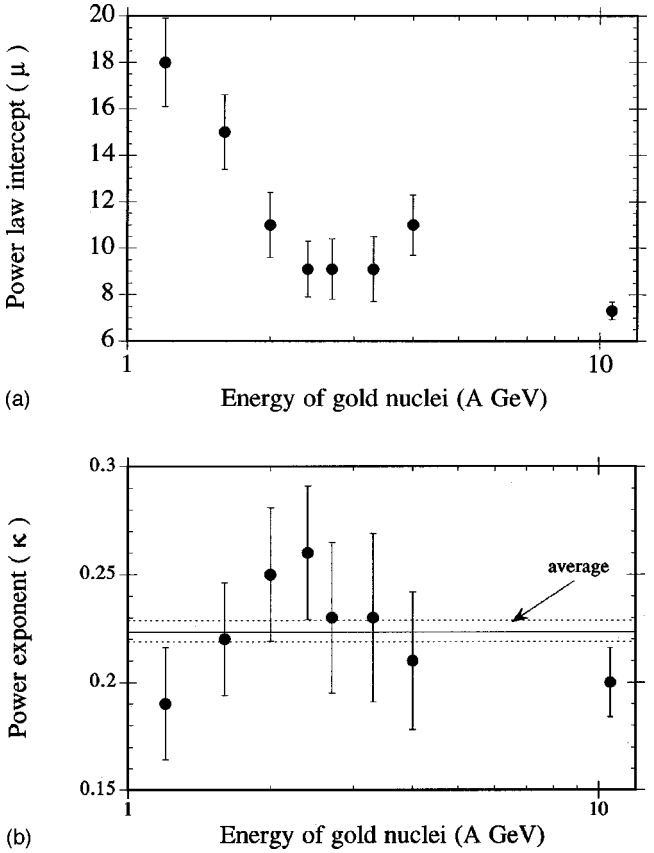

FIG. 21. (a) Values of intercept, μ and (b) exponent, κ, from Eq. (17) for charge pickup as a function of energy.

a representation of the data in this energy range as a simple power law.

E. Plus 2 cross sections

Small numbers of $_{81}$Tl nuclei, plus 2's, have been observed. The cross sections for the production of these nuclei are less than 1.0 mb. It has only been possible to detect a significant number of these rare nuclei due to the larger number of interactions that were obtained during these latest runs at the AGS.

The cross sections were determined using the same procedures as for the plus 1 cross sections, and corrected for the small probability of two interactions resulting in double single charge pickup. The resulting cross sections are plotted in Fig. 22 as a function of the target mass. The large uncertainties prevent any meaningful analysis of trends but it appears that there is a general tendency for the cross sections to increase with A_T, which is consistent with the results found for the plus 1's.

VI. SUMMARY AND DISCUSSION

We have determined the total charge changing cross sections for gold nuclei interacting in a wide range of targets over energies between 0.9 and 10.6 *A* GeV. These cross sections show little if any dependence on energy except for the heaviest targets and at the highest energy. The increases at

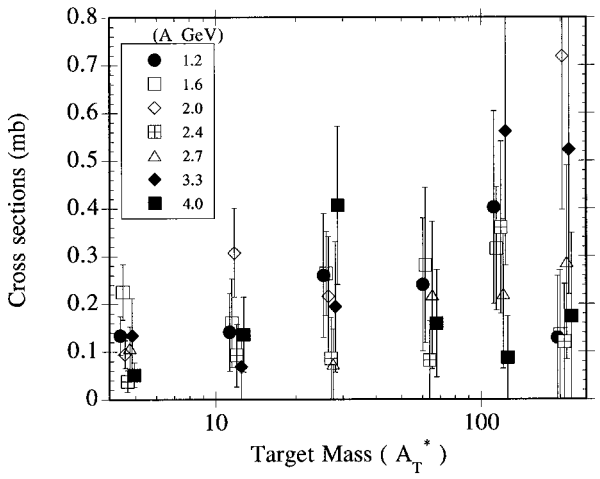

FIG. 22. Cross sections, in mb, for the production of $_{81}$Tl nuclei from $_{79}$Au nuclei at various energies, as a function of target mass number A_T^*.

high energy do not appear to be fully accounted for by simple EMD arguments. The variation of the cross sections with target mass number appear to scale slightly less rapidly than the one-third power that would be expected.

The partial cross sections results obtained here and previously, have been used to derive new expressions for the variations with energy and mass. These expressions are different for hydrogen and heavier targets, but provide better fits to the measured data than previous expressions. At the present time these expression represent the best possible means of predicting those unmeasured cross sections that are required in calculations of the effects of interstellar propagation on the abundance of the heaviest UH cosmic ray nuclei [14].

The nature of the pickup nuclei is not well defined in this experiment. We know that they are stable enough to survive the transit of the charge measuring section of the detector array. At these energies this only places a lower limit on the lifetime of about 10^{-6} s. While we have not measured the mass numbers, previous studies at lower energies suggest that typically there is significant mass loss. The simplest process would be the transformation of one or two neutrons to protons, forming $^{197}_{80}$Hg or $^{197}_{81}$Tl. Both these nuclei have quite adequate lifetimes to traverse the detector array. In the case of ^{197}Hg the nuclei would be stable so long as they were stripped, since the decay is by *K* capture with insufficient energy to allow alternative positron decay. If additional neutrons are lost during the interactions then long lived, or even stable, e.g., ^{196}Hg, nuclei of Hg and Tl can be formed. An experiment to measure the masses of these pickup nuclei, or the numbers of associated neutrons produced during their formation, would help to define the processes that produce them.

The original motivation for these experiments was to study the astrophysical implications of the production of fragments during the propagation of heavy cosmic ray nuclei through interstellar and local matter. It seems unlikely that these pickup processes will be significant to these studies, since the cross sections are so small and the nuclei are prob-

ably not stable. However, it is possible that in certain cases pickup would have to be considered. For example, the production of ^{208}Bi from ^{208}Pb would be possible if there is no mass change, since ^{208}Bi has a long lifetime against *K* capture and might be stable in the cosmic radiation. This could be of interest when good statistical, high resolution, data on the very heavy cosmic ray nuclei becomes available.

ACKNOWLEDGMENTS

This work supported by NASA under Grants No. NASA NAG5-5077 and NAS5-5113. We are indebted to J. Klarmann and Paul Hink for assistance during these runs, and to the staff of the AGS for generous exposures and exceptional help.

[1] W. R. Binns, J. R. Cummings, T. L. Garrard, M. H. Israel, J. Klarmann, E. C. Stone, and C. J. Waddington, Phys. Rev. C **39**, 1785 (1989).
[2] J. R. Cummings, W. R. Binns, T. L. Garrard, M. H. Israel, J. Klarmann, E. C. Stone, and C. J. Waddington, Phys. Rev. C **42**, 2508 (1990); **42**, 2530 (1990).
[3] C. J. Waddington, W. R. Binns, J. R. Cummings, T. L. Garrard, B. W. Gauld, L. Y. Geer, J. Klarmann, and B. S. Nilsen, Nucl. Phys. **A566**, 427c (1994).
[4] B. S. Nilsen, C. J. Waddington, W. R. Binns, J. R. Cummings, T. L. Garrard, L. Y. Geer, and J. Klarmann, Phys. Rev. C **50**, 1065 (1994).
[5] B. S. Nilsen, C. J. Waddington, J. R. Cummings, T. L. Garrard, and J. Klarmann, Phys. Rev. C **52**, 3277 (1995).
[6] L. Y. Geer, J. Klarmann, B. S. Nilsen, C. J. Waddington, W. R. Binns, J. R. Cummings, and T. L. Garrard, Phys. Rev. C **52**, 334 (1995).
[7] S. E. Hirzebruch, E. Becker, G. Huntrup, T. Streibel, E. Winkel, and W. Heinrich, Phys. Rev. C **51**, 2085 (1995).
[8] C. J. Waddington, J. R. Cummings, B. S. Nilsen, and T. L. Garrard, Astrophys. J. **519**, 214 (1999).
[9] S. P. Ahlen, Rev. Mod. Phys. **52**, 121 (1980).
[10] S. P. Ahlen, Phys. Rev. A **25**, 1856 (1982).
[11] C. J. Waddington, D. J. Fixsen, H. J. Crawford, P. J. Lindstrom, and H. H. Heckman, Phys. Rev. A **34**, 3700 (1986).
[12] M. L. Cherry *et al.*, Z. Phys. C **62**, 25 (1994).
[13] Y. D. He, Ph.D. thesis, University of California, Berkeley, 1993.
[14] A. J. Westphal, P. B. Price, B. A. Weaver, and V. G. Afanasiev, Nature (London) **396**, 50 (1998).